Dedicated to Academician Aureliu Săndulescu's 80th Anniversary

COLD NUCLEAR PHENOMENA AND COLLISIONS BETWEEN TWO NON-COPLANAR NUCLEI

MANIE BANSAL, RAJ K. GUPTA

Department of Physics, Panjab University, Chanigarh-160014, India
E-mail: rajkgupta.chd@gmail.com

Received September 16, 2011

Fusion, fission and cluster radioactivity are predicted as cold nuclear phenomena, *prior* to experiments, on the basis of the quantum mechanical fragmentation theory. The fundamental result of the theory is the role of (spherical) closed shell effects of one or both the reaction partners for fusion, or decay products for fission and cluster radioactivity. Also, not only that deformed nuclei are used in fusion experiments, not precluded by the theory, and high neutron multiplicity fission data is observed to be associated with hyper-deformation of the fission fragments, more recently, it is shown that static deformations of nuclei also play an important role in the interpretation of available cluster radioactivity data on the basis of the dynamical preformed cluster model. In view of such results, the role of deformation and orientation effects of the two colliding nuclei is studied here for the colliding nuclei to be in the same plane (co-planar) or different planes (non-coplanar). The aim is to look for the best cold reaction valleys for the synthesis of new and superheavy elements, using non-coplanar collisions, in future experiments. The illustrative examples are the excited compound nuclei $^{286}112^{*}$ and $^{292}114^{*}$.

Key words: Cold fusion, cold fission, cluster radioactivity, quantum mechanical fragmentation theory, cold reaction valleys, deformed-oriented nuclei, non-coplanar collisions, superheavy nuclei.

1. INTRODUCTION

Cold nuclear processes are the cluster radioactivity, cold fission and cold fusion of nuclei for synthesizing new and superheavy elements, predicted for the first time in early 1974–75 by one of us (Raj Gupta), Aurel Săndulescu, Walter Greiner, and collaborators, *prior* to their being observed experimentally. In view of such a pioneering contribution, this article is dedicated to the 80th Birthday celebrations of our dear friend Professor Dr. Aureliu Emil Săndulescu. May the Almighty give him many more years to be amongst us all.

Rom. Journ. Phys., Vol. 57, Nos. 1–2, P. 18–35, Bucharest, 2011

The theory behind such a unified description of all the three (cold) processes of fission, fusion, and cluster radioactivity is the *dynamical or quantum mechanical fragmentation theory* (QMFT), propounded at the Frankfurt School *prior* to any of these processes being observed experimentally, and developed many fold here at Chandigarh through various students of one of us (RKG). The key result behind the three cold processes is the *shell closure effects* of one or both the reaction partners for fusion or that of the decay products for fission and cluster radioactivity. In QMFT, the role of shell effects (largest for a *spherical* closed or nearly closed shell nucleus) arises through "*cold reaction*" or "*cold decay*" *valleys*, corresponding to the *potential energy minima* in the calculated fragmentation potential. Experimentally, for all the three cold phenomena, one of the reaction partner or decay products is always a *spherical* closed or nearly closed shell nucleus. Apparently, the significance of spherical closed shells raises the question of the role of *deformed* closed shells, and other processes like "hot fusion", "hot fission" and cluster decays from excited states of a nucleus (also, the excited compound nucleus). Evidently, the QMFT predict the three cold processes to be the "most probable", meaning thereby that the above noted "hot" processes are not precluded, but they are less probable, compared to their cold counterparts.

Using the QMFT, fission as a cold phenomenon was described as early as in 1974-75 [1, 2], *prior* to the 'Lohengrin' measurements of 1980-81 which established fission as a cold process. The fission fragment's kinetic energies (velocities), together with the masses and charges, were first measured at ILL Grenoble, using the Lohengrin recoil spectrometer [3, 4]. Remembering that spontaneous fission can be accompanied both *with* or *without* neutron emission, for neutron-less (n=0) fission, the total excitation energy TXE=0, and the total kinetic energies TKE of (different) outgoing fragments are close to the Q-value, $Q_{out} \approx$TKE. Then the fission with highest TKE is termed as "cold fission".

Cluster radioactivity, another spontaneous decay of a nucleus, with emission of nuclei heavier than α-particle but lighter than fission fragments, *not* accompanied by any neutron emission (n=0) and hence a cold process (TXE=0 and Q_{out}=TKE, *i.e.*, zero excitation energy and the energy released as Q-value is completely consumed alone by the kinetic energy of the two fragments, the cluster and daughter nuclei), was predicted on the basis of the QMFT in 1980 [5], once again *prior* to its observation in 1984 [6].

Cold synthesis of new and superheavy elements was also proposed theoretically on the basis of QMFT, back in 1974–75 [7-12]. A method was given for selecting out an "optimum" cold target-projectile combination (in terms of the lowest interaction barrier and largest interaction radius) that lie at the bottom of the *potential energy minima*, referred to as "cold reaction valleys" or "cold fusion reactions". Cold compound systems were considered to be formed for *all* possible target + projectile combinations, and the ones corresponding to minima are the "cold" and, hence, more probable. Experimentally, though the arguments of lower

excitation energies were being used at Dubna to select out reaction partners, cold fusion was for the first time observed at GSI in 1994 [13-16] where enhanced fusion cross-sections were observed in reactions with 1n or 2n emission (low TXE), compared to (hot) fusion reactions with emission of 3n to 5n (high TXE). In terms of the incident center-of-mass energies $E_{c.m.}$, low-excitation energies mean below-the-barrier energies. It is relevant to mention here that all the trans-actinides ($Z > 103$) are synthesized since 1975 using only, what can be termed as the "cold fusion reactions" predicted on the basis of the QMFT.

The fact that cold nuclear phenomena evaded detection for such a long time stems from their being of "rare" nature, *i.e.*, occur with much smaller branching ratios *w.r.t.* other known and well observed phenomena. This means to say that these processes are masked by other competing processes, like the cluster radioactivity is masked by the larger number of α-decay events, cold fission by fragments of various other kinetic energies/velocities (hot and/or bimodal fission) and cold fusion by their specific choice of target-projectile combinations, incident bombarding energies and angular momenta. Note that the actual neutron-less (n=0) fission, an equivalent of cluster radioactivity, was observed much later in 1994 at Oak Ridge, where both the neutron-less (n=0) as well as high neutron multiplicity (n=6-10) fissions were observed [17]. This established the "cold" (TXE=0) and "hot" (TXE≠0) fission, as well as the "bi-modal" fission (fission with two different kinetic energy distributions), first observed in 1986 [18]. The observed high neutron multiplicity fission in these experiments is also associated with hyper-deformation of the fission fragments at the scission configuration [19], since the TXE ($=Q_{out}$ - TKE) can go into not only the internal excitation of the fragments but also in their deformation degree of freedom. This hyper-deformation mode is apparently the low TKE (or TXE≠0), hot deformed fission, that was first observed in 1992 at ILL [20]. More recently, the static deformations (and cold "optimum" orientations) of decay fragments are also found to play an important role in spontaneous cluster radioactive decays [21-23].

In this article, we extend our study of the cold phenomena to collisions between two deformed and oriented nuclei, lying in two different planes (non-coplanar nuclei), for reasons of planning future experiments using radioactive nuclear beams (RNB) and targets (RNT). Not much effort has gone in this direction for the QMFT, except for obtaining the nuclear proximity potential for collisions between two symmetric or asymmetric mass, deformed and non-coplanar (as well as co-planar) nuclei [24]. The QMFT, extended to include the effects of both the deformations and orientations of nuclei for both the co-planar and non-coplanar configurations [25], is briefly described in Section 2, and the results of our calculations for the cold fusion of non-coplanar nuclei in Section 3. Specifically, we consider the, so-called, "hot" fusion reactions forming the excited compound systems $^{286}112^{*}$ and $^{292}114^{*}$. In fact, as per QMFT, the "hot" fusion reactions are also the cold fusion reactions. Finally, a brief summary and discussion of our

results is presented in Section 4. For more details on cold nuclear phenomena, we refer the reader to various reviews of one of us (RKG) and collaborators in the very recent books [26, 27], edited alone or with Walter Greiner.

2. THE QUANTUM MECHANICAL FRAGMENTATION THEORY FOR DEFORMED AND ORIENTED NUCLEI

2.1. FRAGMENTATION POTENTIAL

The QMFT [1, 2, 8-12, 25-27] introduces the coordinates of mass and charge asymmetries $\eta=(A_1-A_2)/(A_1+A_2)$ and $\eta_Z=(Z_1-Z_2)/(Z_1+Z_2)$, the relative separation R, the deformation $\beta_{\lambda i}$, λ=2, 3 and 4, the quadrupole, octupole and hexadecapole deformations of two nuclei (i=1, 2), the two orientation angles θ_i and azimuthal angle ϕ between the principal planes of two nuclei, and writes the fragmentation potential as

$$V_R(\eta,\eta_Z,R)=-\sum_{i=1}^{2}B_i(A_i,Z_i,\beta_{\lambda i})+V_C(R,Z_i,\beta_{\lambda i},\theta_i,\phi)+V_P(R,A_i,\beta_{\lambda i},\theta_i,\phi), \quad (1)$$

For coplanar nuclei, $\phi = 0^0$, and for spherical-plus-deformed nuclear system, only one orientation angle θ is enough, referring to the rotationally symmetric deformed nucleus. In Eq. (1), B_i are the binding energies, taken from Möller *et al.* [28] for $Z \geq 8$ (except otherwise stated) and from experiments [29] for $Z < 8$.

For the $\phi = 0^0$ case, the Coulomb potential for two non-overlapping nuclei

$$V_C=\frac{Z_1Z_2e^2}{R}+3Z_1Z_2e^2\sum_{\lambda,i=1}^{2}\frac{1}{2\lambda+1}\frac{R_i^{\lambda}(\alpha_i)}{R^{\lambda+1}}Y_{\lambda}^{(0)}(\theta_i)\left[\beta_{\lambda i}+\frac{4}{7}\beta_{\lambda i}^2Y_{\lambda}^{(0)}(\theta_i)\right] \quad (2)$$

with,

$$R_i(\alpha_i)=R_{0i}\left[1+\sum_{\lambda}\beta_{\lambda i}Y_{\lambda}^{(0)}(\alpha_i)\right] \quad (3)$$

and $R_{0i}=1.28A_i^{1/3}-0.76+0.8A_i^{-1/3}$ for the axially symmetric shapes, and the nuclear proximity potential

$$\begin{aligned} V_P &= f\,(shape,\ geometry)\ \Phi(s_0) \\ &= 4\pi\,\overline{R}\ \gamma\ b\ \Phi(s_0) \end{aligned} \quad (4)$$

where $\overline{R}$ is the mean curvature radius, characterizing the points of closest approach in terms of the minimum separation distance s_0 for nuclei lying in the same plane,

$\gamma = 0.9517\ [1 - 1.7826\{(N - Z)/A\}^2]$ (in MeV fm^{-2}), the specific surface energy constant, $b = 0.99$ fm, the nuclear surface thickness, and the universal function $\Phi(s_0)$, which depends only on s_0, is

$$\Phi\left(s_0\right)=\begin{cases} -\dfrac{1}{2}(s_0-2.54)^2-0.0852(s_0-2.54)^3 & \text{for } s\le 1.2511 \\ -3.437\exp\left(-\dfrac{s_0}{0.75}\right) & \text{for } s\ge 1.2511 \end{cases} \tag{5}$$

Here, the minimized separation distance s_0, in units of b, for coplanar nuclei is defined (see Fig. 1), as

$$s_0 = R - X_1 - X_2 = R - R_1(\alpha_1)\cos(\theta_1 - \alpha_1) - R_2(\alpha_2)\cos(180 + \theta_2 - \alpha_2) \tag{6}$$

with the minimization conditions

$$\tan(\theta_1 - \alpha_1) = -\frac{R_1'(\alpha_1)}{R_1(\alpha_1)}, \qquad \tan(180 + \theta_2 - \alpha_2) = -\frac{R_2'(\alpha_2)}{R_2(\alpha_2)} \tag{7}$$

Here, $R_i'(\alpha_i)$ are the first-order derivatives of $R_i(\alpha_i)$ with respect to α_i. For more details, see Refs. [25, 30].

We use the same formalism as above for non-coplanar nuclei ($\phi \neq 0^0$), but replace for the out-of-plane nucleus (i = 1 or 2) the corresponding radius parameter $R_i(\alpha_i)$ with its projected radius parameter $R_i^P(\alpha_i)$ in both the Coulomb and proximity potentials (2) and (4). For the proximity potential, it enters *via* the definitions of

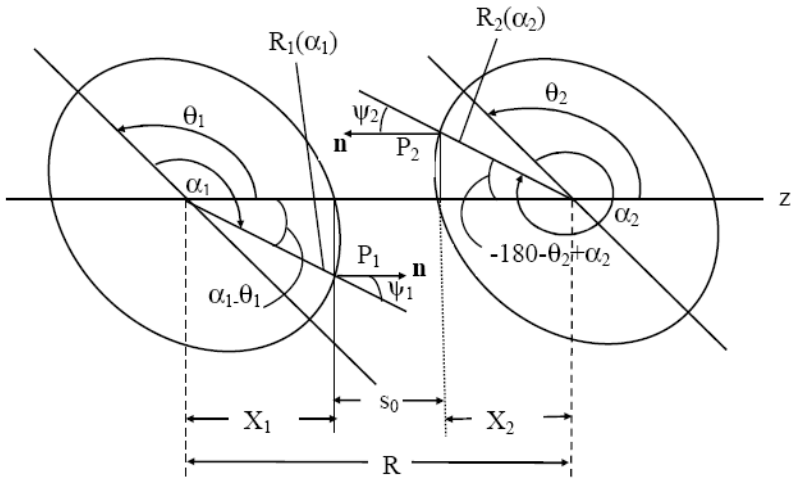

Fig. 1 – Schematic configuration of any two axially symmetric, deformed, oriented nuclei, lying in the same plane ($\phi = 0^0$), based on Fig. 1 in [30].

both the mean curvature radius $\overline{R}$ and the shortest distance s_0 (see Ref. [24]). The $R_i^P(\alpha_i)$ is determined by defining, for the out-of-plane nucleus, two principal planes *X'Z'* and *Y'Z'*, respectively, with radius parameters $R_i(\alpha_i)$ and $R_j(\delta_j)$, such that their projections into the plane *XZ* of the other nucleus are (see Fig. 1 in [24])

$$R_i^P(\alpha_i) = R_i(\alpha_i)\cos\phi \qquad (i = 1 \text{ or } 2) \tag{8}$$

and

$$R_j^P(\delta_j) = R_j(\delta_j)\cos(\phi - \delta_j) \qquad (j = i = 1 \text{ or } 2) \tag{9}$$

Then, maximizing $R_j(\delta_j)$ in angle δ_j, we get

$$\begin{aligned} R_i^P(\alpha_i) &= R_i^P(\alpha_i = 0) + R_i^P(\alpha_i \neq 0) \\ &= R_j^P(\delta_j^{\max}) + R_i(\alpha_i \neq 0)\cos\phi \end{aligned} \tag{10}$$

with $\delta_j^{\max}$ given by the condition (for fixed ϕ),

$$\tan(\phi - \delta_j) = -\frac{R_1'(\delta_j)}{R_1(\delta_j)} \tag{11}$$

Apparently, the ϕ-dependence of the projected radius vector $R_j^P(\alpha_i)$ is also contained in maximized $R_j^P(\delta_j^{\max})$. For further details, see Ref. [24]. Then, denoting by V_P^{12} the nuclear proximity potential for the nucleus 1 to be out-of-plane, and by V_P^{21} for the nucleus 2 to be out-of-plane, the effective nuclear proximity potential can be approximated by

$$V_P = \frac{1}{2}\left[V_P^{12} + V_P^{21}\right]. \tag{12}$$

Note, for co-planar and identical (both nuclei same) non-coplanar nuclei $V_P^{12}=V_P^{21}$.

Thus, for fixed *R,* Eq. (1) gives the fragmentation potential $V(\eta)$ where, for fixed orientations θ_i and ϕ, the charges Z_i are fixed by minimizing $V(\eta)$ in the η_Z coordinate. This fixes the deformations $\beta_{\lambda i}$ also. As already mentioned in the Introduction, in QMFT, the compound system is considered to be formed for *all* possible target-projectile combinations and for cold synthesis of new and super-heavy nuclei, we are interested *only* in those target-projectile combinations that lie at the *minima* of the potential energy surface $V(\eta)$ of a given compound nucleus. This information on potential energy minima, called the "cold reaction valleys", is further optimized by the requirements of smallest interaction barrier, largest interaction radius and non-necked (no saddle) nuclear shapes [9], which depends strongly on the deformation and orientation effects [24, 25, 30-32], as discussed in the next sub-section.

2.2. ORIENTATION-DEPENDENT INTERACTION BARRIERS – "COLD ELONGATED" OR "HOT COMPACT" FUSION

For fixed η, Eq. (1) gives, on normalization to the binding energies, the interaction barrier *V(R)*. With the orientation degrees of freedom included, for fixed deformations β_2 and β_4 (in general, β_3=0), the barrier shows, for each ϕ, a distribution in orientation angle θ_i [24, 25, 30-32]. Two situations arise, say, for positive β_2: (i) the barrier is lowest and the interaction radius largest for θ_i close to 0^0 and 180^0, called "cold elongated" fusion barrier, and (ii) the barrier is highest and the interaction radius smallest for θ_i *close* to both 90^0 and 90^0, called "hot compact" fusion [25, 31]. Interestingly, the θ_i-values of the "elongated" and "compact" configurations depend on the sign of β_2 (prolate/oblate) and both sign and magnitude of β_4 deformations [31, 32]. For (prolate) quadrupole deformation (positive β_2) alone or with additional small (including negative) hexadecapole deformation, $\theta_i=0^0$ and 180^0 (nose-to nose, nn or pole-to-pole) or $\theta_1=\theta_2=90^0$ (belly-to-belly, bb or equator-cross), respectively, for "cold elongated" or "hot compact" configuration, but with large (positive) hexadecapole deformation, the two configurations are non-nn or not-bb with θ_i differing by as much as 20^0 from, say, the bb value [31]. Much of these calculations are made for $\phi=0^0$ (co-planar nuclei), and the inclusion of non-zero β_3 values (normally negative, though known for only some nuclei) changes this result significantly, say, not-bb configuration due to large positive β_4 changes back to bb due to negative β_3, and vice-versa, which means acting inverse to the role of β_4 [32]. For collisions between non-coplanar nuclei ($\phi\neq0^0$), only a special case of "hot compact" configuration ($\theta_1=\theta_2=90^0$) of prolate deformed nuclei is studied [24]. It is shown that for $\phi=90^0$, this configuration for negative hexadecapole deformation ($\beta_4<0$) refers to "hot compact", (called, "hugging") and for positive β_4 ($\beta_4>0$) to "cold elongated" (called, "gentle") configuration. The role of ϕ is also studied for this special configuration [24]. The aim of the present study is to generalize this work to other configurations, both in θ_i and ϕ. We concentrate here only on "hot compact" configurations for reasons of including deformation and orientation effects. Note that in experiments both spherical and deformed nuclei are used for synthesizing superheavy nuclei, referred to as cold and hot fusion, respectively, on the basis of excitation energy E^* involved or number of neutrons emitted (E^*~10-20 MeV or 1n-2n emitted for cold and E^*~35-41 MeV or 3n-5n emitted for hot fusion reactions), whereas on the basis of QMFT, both cold and hot configurations refer to "cold reaction valleys".

3. CALCULATIONS AND RESULTS

First of all, we choose a reaction $^{206}Hg+^{80}Ge\rightarrow^{286}112^*$ consisting of two deformed nuclei, one *oblate* (^{206}Hg: β_{21}=–0.008) and another *prolate* (^{80}Ge:

$\beta_{22} = 0.144$), and determine their "*hot compact*" configuration [using Eqs. (7) and (11)] in both the orientation degrees of freedom θ_i, ϕ (denoted θ_{ci}, ϕ_c; I = 1, 2). We find that barrier V_B is *highest* for $\theta_{c1} = 4^0$, $\theta_{c2} = 97^0$ (near-bb configuration for oblate-prolate system) and $\phi_c = 84^0$ (near-orthogonal symmetry axes), illustrated in Fig. 2 where the scattering potentials V(R) are plotted as a function of the three orientation degrees of freedom (θ_1, θ_2 and ϕ), keeping two of them fixed at a time. This is a very (computer) time consuming calculation. This choice of reaction is a case of octupole deformations $\beta_{3i} = 0$, and zero and small-negative hexadecapole

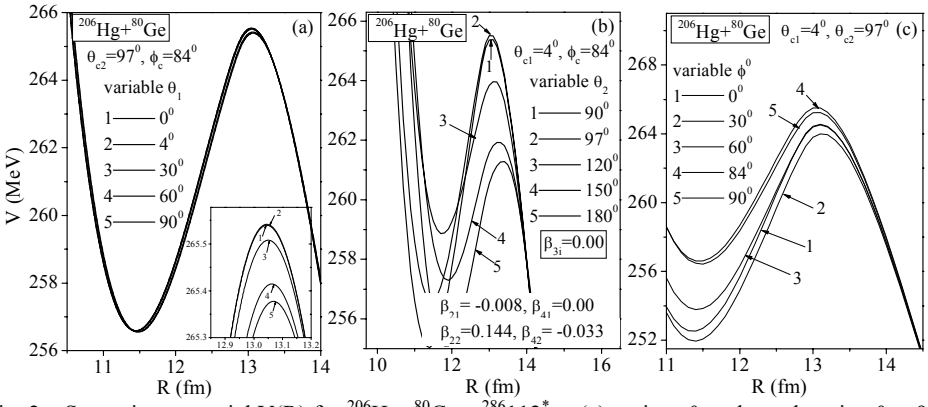

Fig. 2 – Scattering potential V(R) for $^{206}Hg+^{80}Ge \rightarrow ^{286}112^*$ at (a) various θ_1 values, keeping $\theta_{c2}=97^0$ and $\phi_c=84^0$ fixed, (b) various θ_{c2}, keeping $\theta_{c1}=4^0$ and $\phi_c=84^0$ fixed, and (c) various ϕ values, keeping $\theta_{c1}=4^0$ and $\theta_{c2}=97^0$ fixed. The inset in (a) shows that the barrier is highest at $\theta_1 = \theta_{c1}=4^0$.

deformations $\beta_{41} = 0$, $\beta_{42} = -0.033$. As expected [31, 32], we get near-bb compact configuration ($\theta_{c1} = 4^0$, $\theta_{c2} = 97^0$), which in non-coplanar degree of freedom ϕ is hot compact in near-orthogonal configuration ($\phi_c = 84^0$, whereas $\phi_c = 90^0$ refers to orthogonal symmetry axes).

Next, we study the role of deformations β_{2i} on azimuthal angle ϕ for fixed β_{4i}, similar to what was studied in [31] for θ_i in the case of $\phi = 0^0$. Figure 3 shows the variation of barrier height V_B with β_{2i} for the $^{206}Hg+^{80}Ge$ collisions at fixed orientations $\theta_{c1} = 4^0$, $\theta_{c2} = 97^0$, the hot compact orientation angles for ^{206}Hg and ^{80}Ge, respectively. Figure 3 (a) or (b) shows that ϕ_c remains the same ($= 84^0$) for the limiting β_{2i}-values, *i.e.*, $\beta_{21} > -0.02$ and $\beta_{22} > 0.02$ (nearly-prolate and prolate deformations), but changes drastically to $\phi_c = 0^0$ (co-planar configuration) for further negative β_{2i} deformations, *i.e.*, $\beta_{21} < -0.02$ and $\beta_{22} < 0.02$ including all negative values (oblate deformations). This is an interesting result, obtained for the first time. Note that here β_{4i} are fixed ($\beta_{41} = 0$, $\beta_{42} = -0.033$), and different choices of β_{4i} might result in different ϕ_c, as is illustrated in the following in Fig. 4.

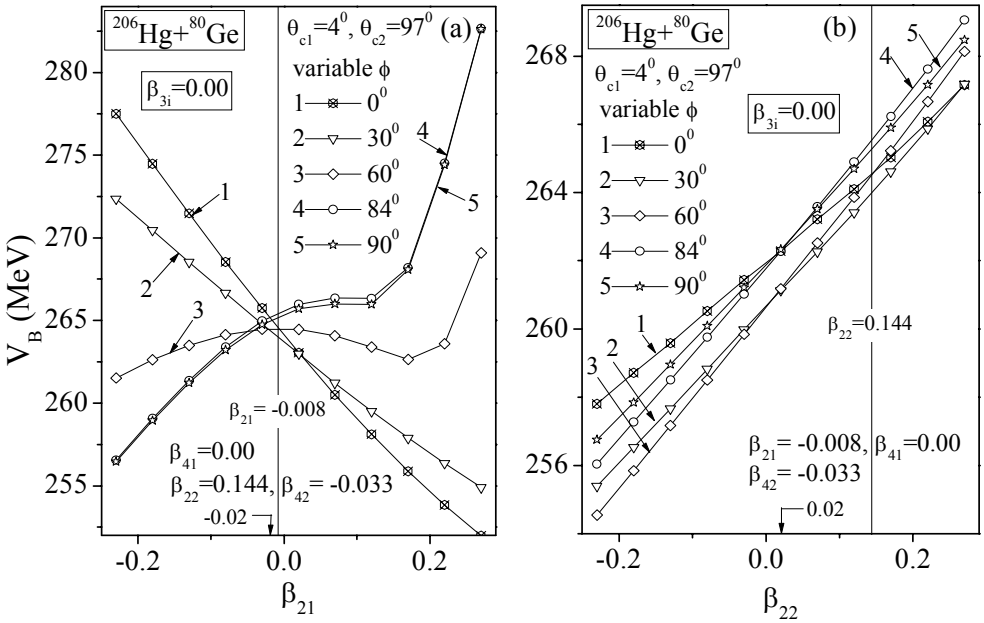

Fig. 3 – The top of the barrier V_B as a function of quadrupole deformation (a) β_{21} (b) β_{22}, for different ϕ values at fixed $\theta_{c1}=4^0$, $\theta_{c2}=97^0$ and $\beta_{41}=0$, $\beta_{42}=-0.033$, calculated for ^{206}Hg+^{80}Ge→^{286}112* reaction. The β_{21} and β_{22} values of ^{206}Hg and ^{80}Ge, respectively, are also marked.

Figure 4 shows the variation of V_B with hexadecapole deformations β_{4i} for the same reaction (^{206}Hg+^{80}Ge) at the fixed compact orientations $\theta_{c1} = 4^0$, $\theta_{c2} = 97^0$, and ϕ varying from 0^0 to 90^0. Only the variation of β_{42}, referring to ^{80}Ge, is studied. We notice that for large positive β_{42} ($\beta_{42} >> 0$), the compact configuration is obtained at $\phi_c = 60^0$ whereas for large negative β_{42} ($\beta_{42} << 0$), $\phi_c = 90^0$. Since $\beta_{42} = -0.033$ for the nucleus under consideration, ϕ_c remains the same as before ($=84^0$) in a small range ($-0.057 < \beta_{42} < -0.010$) of its neighborhood. Note that we are considering here an oblate-prolate pair of nuclei. Interestingly, the above result of $\phi_c = 60^0$ for $\beta_{42} >> 0$ changing to $\phi_c = 90^0$ for $\beta_{42} << 0$ supplements the same result obtained for prolate-prolate pair of nuclei [24]. This means to say that the role of the sign of quadrupole deformation (oblate/ or prolate) is reflected only in the determination of compact orientation angle θ_{ci} and not for ϕ_c. It may be reminded that all the above results of Figs. 2–4 are for the case of $\beta_{3i} = 0$. The case of $\beta_{3i} \neq 0$ is investigated further in the following.

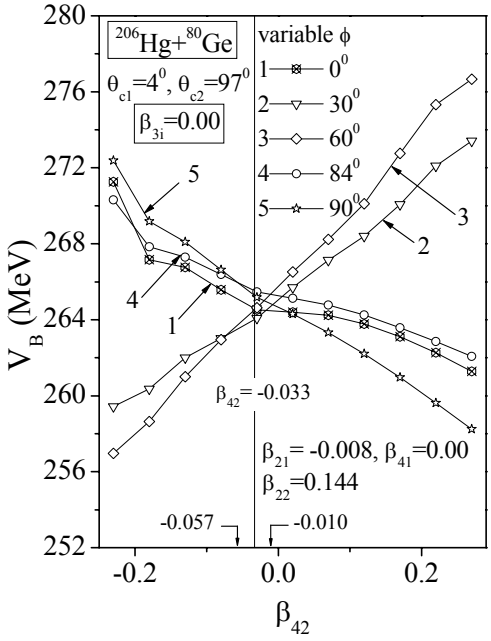

Fig. 4 – The barrier height V_B as a function of hexadecapole deformation β_{42} for different ϕ angles for ^{206}Hg+^{80}Ge→^{286}112* reaction at fixed compact orientations $\theta_{c1}=4^0$and $\theta_{c2}=97^0$. The β_{42} value of ^{80}Ge is also marked.

In order to see the effect of β_{3i} on ϕ_c, we choose the reaction ^{226}Ra+^{60}Cr→ ^{286}112* where $\beta_{31}=-0.108$, $\beta_{41}=0.112$ for ^{226}Ra, and $\beta_{32}=0$, $\beta_{42}=-0.021$ for ^{60}Cr. Since this is a case of one nucleus with large positive β_4-value ($\beta_{41}=0.112$ for ^{226}Ra), the compact orientations are those of not-bb ($\theta_{c1}=66^0$, $\theta_{c2}=98^0$) for the case $\beta_{31}=0$, respectively, with $\phi_c=90^0$ and 60^0 for negative and positive (including zero) β_{41} values, as depicted in Fig. 5(a). Knowing that addition of β_3 acts (inverse) to the role of β_4, *i.e.*, addition of negative β_3 compensates for the effect of positive β_4 and vice-versa [32], the not-bb configuration in the present study becomes bb or near bb compact ($\theta_{c1}=90^0$, $\theta_{c2}=96^0$) on addition of negative β_{31} ($\beta_{31}=-0.108$ for ^{226}Ra), but ϕ_c remain the same ($=90^0$) for negative (including zero) β_{41}, but with a small change (from $\phi_c=60^0$ to 52^0) for $\beta_{41}>>0$. Note that ϕ_c is still $=60^0$ in the small range of $\beta_{41}>0$ ($\beta_{41}=0.036$ to 0.07), which is smaller than the β_{41} value (=0.112) for ^{226}Ra, as presented in Fig. 5(b). The change in ϕ_c due to the sign of β_3 is also studied here in Fig. 5(c) for the case of large positive $\beta_{41}=0.112$. We notice that, with in reasonable limits of both positive and negative β_{31}-values, ϕ_c is independent of both the sign and magnitude of β_{31}, *i.e.*, $\phi_c=52^0$.

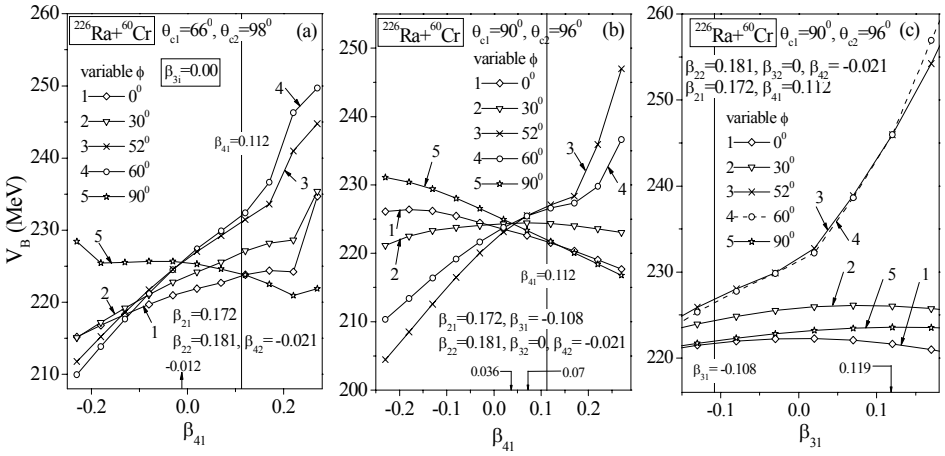

Fig. 5 – The barrier height V_B for the reaction ^{226}Ra+^{60}Cr→^{286}112* as a function of deformations (a) β_{41} taking β_{31} = 0, with the corresponding $\theta_{c1,}$ θ_{c2}, (b) β_{41} taking β_{31} = –0.108, with the corresponding $\theta_{c1,}$ θ_{c2}, (c) β_{31} with $\theta_{c1,}$ θ_{c2} fixed for β_{31} = –0.108, varying in each case the azimuthal angle ϕ from 0^0 to 90^0. The β_{41} and β_{31} value of ^{226}Ra are also marked as vertical lines.

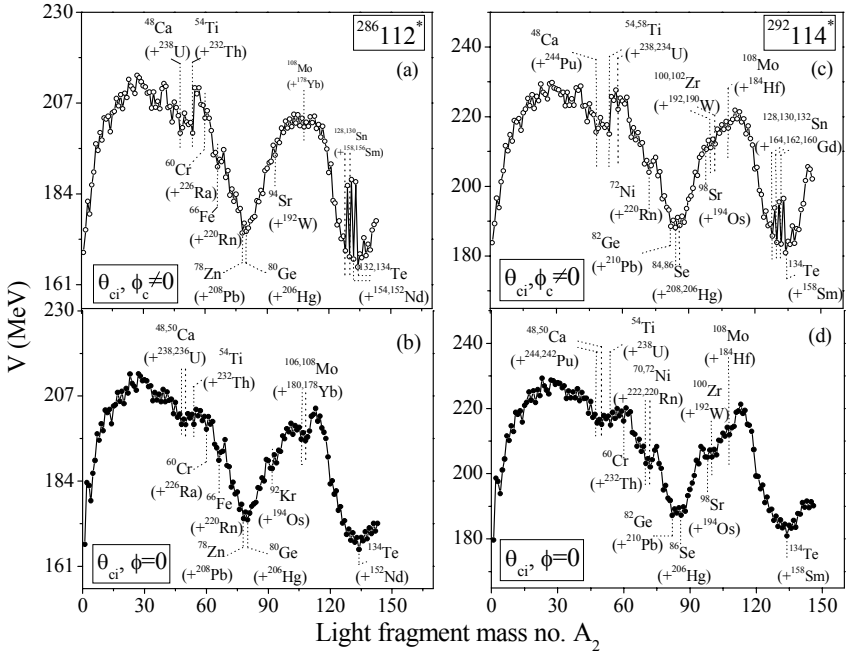

Fig. 6 – Fragmentation potentials $V(A_2)$ for the hot compact configurations of different target-projectile combinations, having deformations up to hexadecapole deformations (β_2–β_4) and lying [(b) and (d)] in one plane (ϕ = 0^0) or [(a) and (c)] in two planes ($\phi_c \neq 0^0$), forming the excited compound systems ^{286}112* and ^{292}114*. The calculations for ϕ = 0^0 are based on [31].

Next, for a given compound nucleus, we calculate the fragmentation potential V(η) for the "compact hot" orientations θ_{ci} and ϕ_c of all possible target-projectile (t-p) combinations forming the compound systems $^{286}112^*$ and $^{292}114^*$. This is given in Fig. 6, for both the cases of $\phi_c = 0$ and $\phi_c \neq 0$, calculated at $R = R_B$ for compact θ_{ci} of each t-p combination (η value). Such a calculation needed large computer time, since this meant searching for a configuration with the shortest distance s_0 for each possible pair of the oriented colliding nuclei, consisting of both spherical + (prolate/ oblate) deformed and deformed + deformed t-p combinations. We made this search in steps of $\Delta\theta = 1^0$ and $\Delta\phi = 2^0$. The deformation effects are included up to hexadecapole ($\beta_2 - \beta_4$) deformations. We notice in Fig. 6 that, in each case, in addition to a minimum at the experimentally studied reaction $^{48}Ca + ^{238}U$ [33] and ^{244}Pu [34], a number of other reaction valleys (minima) occur, including the one at an isotope of Pb, used for "cold fusion" reactions [13, 14]. The resulting t-p combinations are listed in Table 1, together with their other characteristics, such as the deformations, barriers V_B, R_B, and compact orientations θ_{ci} and ϕ_c.

Table 1

Target-projectile (A_1, A_2) combinations for compound systems (CS) $^{286}112^*$ and $^{292}114^*$ referring to potential energy minima in V(η) for hot compact configurations in both θ_{ci} and ϕ_c, and other characteristics, for the two nuclei lying in the same plane ($\phi = 0$, based on [31]) or in two different planes ($\phi_c \neq 0$).

CS	Reactions (A_1+A_2)	Deformations β_{21}	β_{31}	β_{41}	β_{22}	β_{32}	β_{42}	Case	Barrier V_B	R_B	Compact θ_1	θ_2	ϕ
$^{286}112$	$^{238}U + ^{48}Ca$	0.215	0.0	0.093	0.0	0.0	0.0	$\phi=0^0$	195.43	12.67	72^0	s	0^0
								$\phi\neq0^0$	195.41	12.70	72^0	s	0^0*
	$^{236}U+^{50}Ca$	0.215	0.0	0.102	0.0	–0.015#	0.0	$\phi=0^0$	194.74	12.72	71^0	s	0^0
	$^{232}Th+^{54}Ti$	0.207	0.0	0.108	0.0	0.0	0.0	$\phi=0^0$	208.98	12.78	68^0	s	0^0
								$\phi\neq0^0$	208.976	12.8	68^0	s	0^0*
	$^{226}Ra+^{60}Cr$	0.172	–0.108	0.112	0.181	0.0	–0.021	$\phi=0^0$	221.73	12.78	90^0	96^0	0^0
								$\phi\neq0^0$	226.889	12.5	90^0	96^0	52^0
	$^{220}Rn+^{66}Fe$	0.111	–0.146	0.081	0.027	0.0	0.0	$\phi=0^0$	230.11	13.13	90^0	90^0	0^0
								$\phi\neq0^0$	231.323	13.10	90^0	90^0	36^0
	$^{208}Pb+^{78}Zn$	0.0	–0.013	0.0	0.089	0.0	0.003	$\phi=0^0$	253.57	13.15	s	90^0	0^0
								$\phi\neq0^0$	253.799	13.10	0^0	90^0	64^0
	$^{206}Hg+^{80}Ge$	–0.008	0.0	0.0	0.144	0.0	–0.033	$\phi=0^0$	264.57	13.10	4^0	97^0	0^0
								$\phi\neq0^0$	265.511	13.00	4^0	97^0	84^0
	$^{194}Os+^{92}Kr$	0.145	0.0	–0.082	0.228	0.0	–0.019	$\phi=0^0$	288.02	12.73	86^0	97^0	0^0
	$^{192}W+^{94}Sr$	0.155	0.0	–0.082	0.255	0.0	0.001	$\phi\neq0^0$	301.888	12.50	85^0	90^0	86^0
	$^{180}Yb+^{106}Mo$	0.279	0.0	–0.098	0.361	0.0	–0.002	$\phi=0^0$	317.48	12.27	89^0	95^0	0^0
	$^{178}Yb+^{108}Mo$	0.279	0.0	–0.087	0.333	0.0	–0.027	$\phi=0^0$	316.71	12.31	89^0	95^0	0^0

Table 1 (continued)

								$\phi\neq0^0$	322.733	12.10	89^0	95^0	88^0
	$^{158}Sm+^{128}Sn$	0.279	0.0	0.082	0.0	0.0	0.0	$\phi\neq0^0$	319.151	13.10	90^0	s	0^0*
	$^{156}Sm+^{130}Sn$	0.279	0.0	0.098	0.0	0.0	0.0	$\phi\neq0^0$	318.676	13.10	87^0	s	0^0*
	$^{154}Nd+^{132}Te$	0.27	0.0	0.114	0.0	0.0	0.0	$\phi\neq0^0$	320.137	13.10	78^0	s	0^0*
	$^{152}Nd+^{134}Te$	0.262	0.0	0.128	0.0	0.0	0.0	$\phi=0^0$	319.83	13.17	74^0	s	0^0
								$\phi\neq0^0$	319.836	13.2	74^0	s	0^0*
$^{292}114$	$^{244}Pu+^{48}Ca$	0.224	0.0	0.062	0.0	0.0	0.0	$\phi=0^0$	199.42	12.65	90^0	s	0^0
								$\phi\neq0^0$	199.40	12.60	90^0	s	0^0*
	$^{242}Pu+^{50}Ca$	0.224	0.0	0.071	0.0	–0.015#	0.0	$\phi=0^0$	198.47	12.71	89^0	s	0^0
	$^{238}U+^{54}Ti$	0.215	0.0	0.093	0.0	0.0	0.0	$\phi=0^0$	212.77	12.81	72^0	s	0^0
								$\phi\neq0^0$	212.754	12.8	72^0	s	0^0*
	$^{234}U+^{58}Ti$	0.215	0.0	0.11	–0.105	0.0	–0.011	$\phi\neq0^0$	215.695	12.5	70^0	180^0	56^0
	$^{232}Th+^{60}Cr$	0.207	0.0	0.108	0.181	0.0	–0.021	$\phi=0^0$	228.17	12.71	71^0	98^0	0^0
	$^{222}Rn+^{70}Ni$	0.137	–0.132	0.100	0.027	0.0	0.0	$\phi=0^0$	246.74	13.18	90^0	92^0	0^0
	$^{220}Rn+^{72}Ni$	0.111	–0.146	0.081	0.053	0.0	0.009	$\phi=0^0$	246.27	13.21	90^0	91^0	0^0
								$\phi\neq0^0$	248.131	13.10	90^0	91^0	38^0
	$^{210}Pb+^{82}Ge$	0.0	0.0	0.008	0.053	0.0	0.001	$\phi=0^0$	267.53	13.32	52^0	91^0	0^0
								$\phi\neq0^0$	268.765	13.30	52^0	91^0	52^0
	$^{208}Pb+^{84}Ge$	–0.008	0.0	0.0	0.053	0.0	–0.007	$\phi\neq0^0$	277.799	13.30	6^0	91^0	72^0
	$^{206}Hg+^{86}Se$	–0.008	0.0	0.0	0.125	0.0	0.006	$\phi=0^0$	278.69	13.22	5^0	91^0	0^0
								$\phi\neq0^0$	280.102	13.10	5^0	91^0	62^0
	$^{194}Os+^{98}Sr$	0.145	0.0	–0.082	0.357	0.0	0.056	$\phi=0^0$	305.43	12.63	86^0	90^0	0^0
								$\phi\neq0^0$	310.934	12.4	86^0	90^0	82^0
	$^{192}W+^{100}Zr$	0.155	0.0	–0.082	0.358	0.0	0.039	$\phi=0^0$	313.18	12.62	85^0	90^0	0^0
								$\phi\neq0^0$	319.124	12.4	85^0	90^0	82^0
	$^{190}W+^{102}Zr$	0.173	0.0	–0.097	0.369	0.0	–0.097	$\phi\neq0^0$	320.108	12.3	86^0	90^0	86^0
	$^{184}Hf+^{108}Mo$	0.260	0.0	–0.128	0.333	0.0	–0.027	$\phi=0^0$	326.09	12.3	90^0	94^0	0^0
								$\phi\neq0^0$	330.840	12.1	90^0	94^0	90^0
	$^{164}Gd+^{128}Sn$	0.301	0.0	0.029	0.0	0.0	0.0	$\phi\neq0^0$	329.594	13.1	90^0	s	0^0*
	$^{162}Gd+^{130}Sn$	0.291	0.0	0.042	0.0	0.0	0.0	$\phi\neq0^0$	328.914	13.1	90^0	s	0^0*
	$^{160}Gd+^{132}Sn$	0.28	0.0	0.065	0.0	0.0	0.0	$\phi\neq0^0$	327.970	13.1	90^0	s	0^0*
	$^{158}Sm+^{134}Te$	0.279	0.0	0.082	0.0	0.0	0.0	$\phi=0^0$	330.05	13.16	0^0	s	0^0
								$\phi\neq0^0$	330.025	13.2	90^0	s	0^0*

*Case of one reaction partner being a spherical nucleus.

#Taken to be equal to zero for the calculations in case of $\phi=0^0$.

We notice in Fig. 6 and Table 1 that with the inclusion of ϕ degree of freedom, some minima (t-p combinations) are washed out, *i.e.*, $^{236}U+^{50}Ca$, $^{194}Os+^{92}Kr$, $^{180}Yb+^{106}Mo\rightarrow^{286}112$, and $^{242}Pu+^{50}Ca$, $^{232}Th+^{60}Cr$, $^{222}Rn+^{70}Ni\rightarrow^{292}114$ occur only for $\phi = 0^0$ case, and some new minima are obtained, *i.e.*, $^{192}W+^{94}Sr$,

^{158,156}Sm+^{128,130}Sn, ^{154}Nd+^{132}Te→^{286}112, and ^{234}U+^{58}Ti, ^{208}Hg+^{84}Se, ^{190}W+^{102}Zr, ^{164,162,160}Gd+^{128,130,132}Sn→^{292}114 occur only if $\phi \neq 0^0$. The other minima in Table 1 occur in both the case of co-planar ($\phi = 0^0$) and non-coplanar ($\phi \neq 0^0$) collisions.

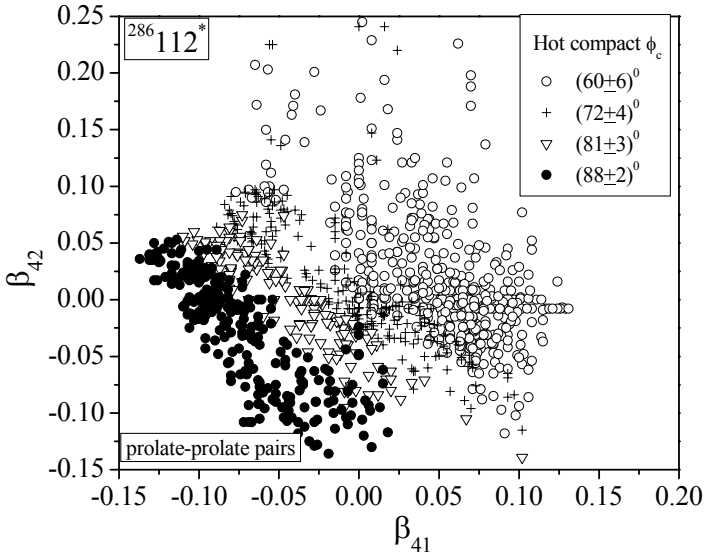

Fig. 7 – Hot compact azimuthal angle ϕ_c as functions of hexadecapole deformations β_{41} and β_{42}, illustrated for prolate-prolate deformed pairs of colliding nuclei forming ^{286}112* compound system.

The role of large positive hexadecapole deformations ($\beta_{41} >> 0$ or $\beta_{42} >> 0$) for prolate-prolate deformed pairs of nuclei, is also evident in Table 1, in changing the compact bb (or near-bb) configurations with $\phi_c \approx 90^0$ for zero or negative hexadecapole deformations ($\beta_{41} \leq 0$ or $\beta_{42} \leq 0$), to compact not-bb with $\phi_c \approx 60^0$ for large positive hexadecapole deformations. This means that $\phi_c \approx 90^0$ for $\beta_{41} \leq 0$ or $\beta_{42} \leq 0$ changes to $\phi_c \approx 60^0$ for $\beta_{41} >> 0$ or $\beta_{42} >> 0$. This is illustrated more clearly in Fig. 7 for ^{286}112*, where ϕ_c (calculated in steps of $\pm 2^0$) are plotted as functions of both β_{41} and β_{42}. We have made similar calculations for other systems, like ^{246}Bk* and ^{292}114*, and find that the above result is (nearly) independent of mass and charge of the compound nucleus. For oblate-oblate pairs of nuclei we find that for zero or negative hexadecapole deformations ($\beta_{41} \leq 0$ or $\beta_{42} \leq 0$) $\phi_c = 0^0$, as expected, but not enough cases with large positive β_4 deformations are available to show these results here. On the other hand, for the compact orientations θ_{ci}, we already know from [31] that the differences between the compact bb and compact not-bb are ~20^0, as is illustrated in Fig. 8 (based on Ref. [35]), and that the orientation of one nucleus is independent of the orientation of the other colliding nucleus.

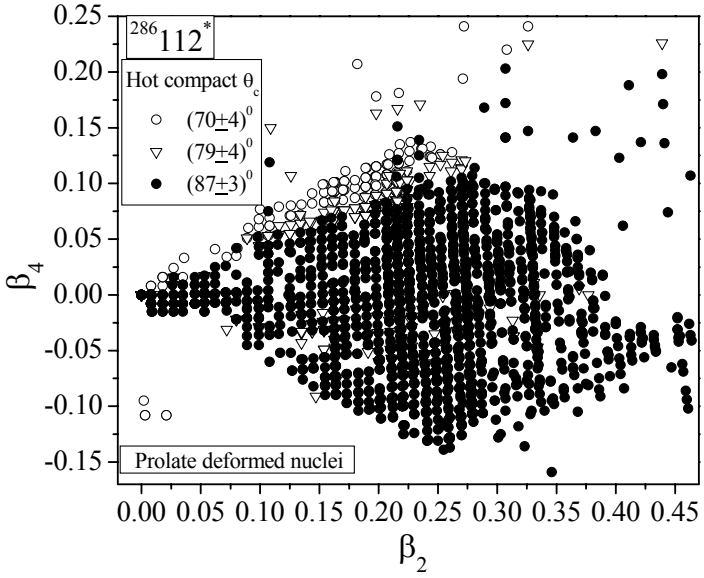

Fig. 8 – Same as Fig. 7, but for hot compact orientation angles θ_{ci} as functions of quadrupole and hexadecapole deformations β_2 and β_4, based on Fig. 7.2 in [35].

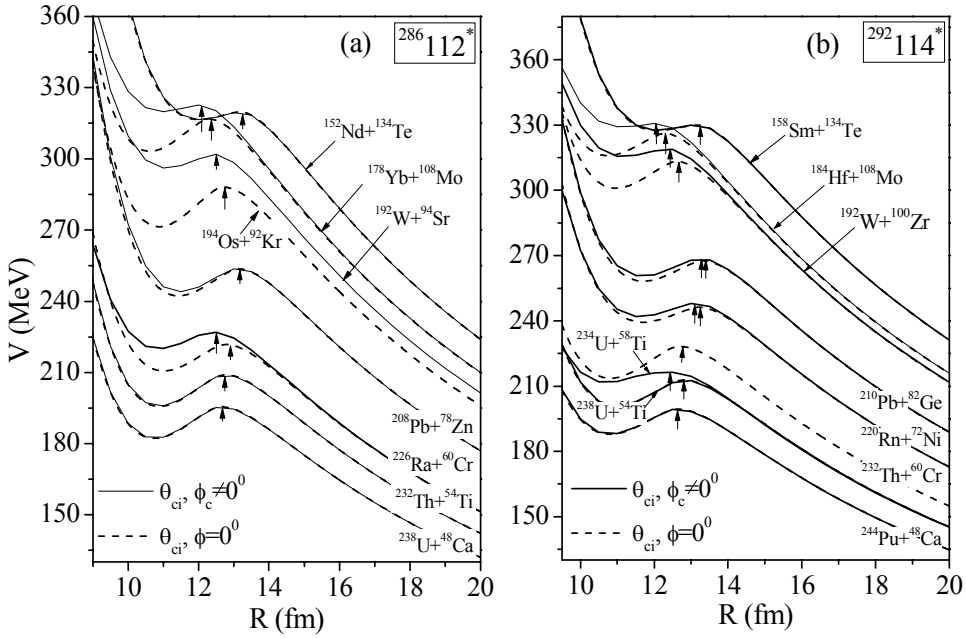

Fig. 9 – Scattering potentials for different t-p combinations listed in Table 1, referring to minima in hot compact fusion potential energy surfaces of Fig. 6. Arrows indicate barrier position.

We further find in Table 1 that, in some cases, the non-zero β_3 ($\beta_3 \neq 0$) also plays an important role like, *e.g.*, in reaction $^{226}Ra+^{60}Cr \rightarrow ^{286}112^*$, the ^{226}Ra has large $+\beta_4$ but, because of $\beta_3 \neq 0$, it behaves as one with small or $-\beta_4$, as already discussed above.

Finally, remembering that the potential energy minima in Table 1 refer to "hot compact" fusion configurations in orientation degrees of freedom, the best "cold fusion" reaction could next be found by carrying out the optimization requirements of the potential energy minima in terms of the smallest interaction barrier and largest interaction radius. Fig. 9 gives the scattering potentials for a few representative t-p combinations listed in Table 1 for hot compact fusion of compound systems $^{286}112^*$ and $^{292}114^*$, plotted for both the cases of $\phi = 0^0$ and $\phi_c \neq 0^0$. It is apparent from these figures that there are some small changes in barrier heights and positions in going from $\phi = 0^0$ to $\phi_c \neq 0^0$, *i.e.*, for the deformed + deformed t-p combinations. The net result is an increase in height and decrease in position of the barrier, a favorable condition for "hot compact" fusion. However, the barrier is still the lowest for ^{48}Ca induced reactions (case of $\phi = 0^0$, since ^{48}Ca is spherical), and that the next best cold reaction valley is still the ^{54}Ti based reactions on ^{238}U and ^{232}Th actinides for Z=112 and 114, respectively. Such actinide based reactions were planned to be carried out at GSI (Darmstadt), some years back, though ^{54}Ti is also a spherical nucleus. For the deformed + deformed pairs, the apparent choices from Fig. 9 are, respectively, $^{226}Ra+^{60}Cr$ and $^{234}U+^{58}Ti$ for Z=112 and 114 nuclei, in non-coplanar ($\phi_c \neq 0^0$) configurations.

4. SUMMARY AND DISCUSSION OF RESULTS

Cold nuclear phenomena, comprising of cold fission, cluster radioactivity and cold fusion for synthesizing new and superheavy elements, is introduced on the basis of the dynamical or quantum mechanical fragmentation theory (QMFT) that predicted these processes *prior* to their being observed experimentally. The important role is played by the closed shell effects of one or both the decay products in fission and cluster radioactivity or the reaction partners in fusion. In view of the possible role of static deformations and orientations of nuclei, in this paper, we extended the work of QMFT to the collisions of two nuclei lying in two different planes (non-coplanar nuclei), including, of course, the case of co-planar nuclei. In other words, we looked for "cold fusion" reactions, involving both reaction partners as deformed as well as oriented nuclei. Apparently, the role of the magnitudes of multipole deformations, *i.e.*, the quadrupole β_2, octupole β_3 and hexadecapole β_4 deformations, and phenomenon of compactness, *i.e.*, "compact" orientation angles θ_{ci} (i = 1, 2) and azimuthal angle ϕ_c come in to play. We have analyzed here the experimentally synthesized "hot fusion" compound systems

$^{286}112^{*}$ and $^{292}114^{*}$. This means that for a given compound nucleus, we first look for all the possible "compact hot" fusion configurations (target + projectile combinations) with highest barrier and smallest interaction radius, then identify the reaction valleys (potential energy minima), and finally, of these, the "cold fusion" reaction with the smallest interaction barrier and largest interaction radius.

First of all, talking of the "hot compact" configurations for quadrupole β_2 deformed nuclei, just as for compact orientations θ_{ci} for co-planar ($\phi = 0^0$) nuclei, $\phi_c \approx 90^0$ (near-orthogonal) and $=0^0$ (co-planar), respectively, for prolate-prolate and oblate-oblate collisions, independent of the magnitude of β_2 (for $\phi = 0^0$ case, $\theta_{c1} = \theta_{c2} = 90^0$ and 0^0, respectively [31]). Similarly, ϕ_c is independent of both the sign and magnitude of β_{3i}. However, both the sign and the magnitude of hexadecapole deformation β_4 are important for determining ϕ_c. For $\beta_{3i} = 0$, $\phi_c \approx 90^0$ for zero and negative β_{4i} ($\beta_{41} \leq 0$ or $\beta_{42} \leq 0$), and $\approx 60^0$ for large positive β_{4i} ($\beta_{41} >> 0$ or $\beta_{42} >> 0$); (for $\phi = 0^0$ case, $\theta_{c1} = \theta_{c2} = 90^0$ (or $\approx 90^0$) and $\approx 70^0$, respectively [31]). Note that the role of the sign of quadrupole deformation (oblate/ or prolate) is reflected only in the determination of compact orientation angle θ_{ci} and not for ϕ_c. Also, addition of β_3 ($\beta_3 \neq 0$) reverses the role of the sign of β_4, *i.e.*, adding $-\beta_3$ (normally the case) to $+\beta_4$ reverses its action of ($\theta_c = 70^0$, $\phi_c = 60^0$) back to ($\theta_c = 90^0$, $\phi_c = 90^0$), but the same added to $-\beta_4$ ((including zero) does not change either the θ_c or ϕ_c, *i.e.*, remain the same ($= 90^0$, 90^0).

Finally, the calculated fragmentation potentials, using hot compact θ_{ci} for $\phi_c \neq 0$ case, gives for the compound systems $^{286}112^{*}$ and $^{292}114^{*}$, the various cold reaction valleys, which always include ^{48}Ca, ^{54,58}Ti, ^{60}Cr + deformed actinides, the ^{208,210}Pb valley, and many other spherical + deformed and deformed + deformed reaction partners. An interesting result of going from $\phi = 0^0$ to $\phi_c \neq 0^0$ case is an increase in height and decrease in position of the barrier, a favorable condition for "hot compact" fusion. In any case, some of these target + projectiles are the same as were obtained for $\phi = 0^0$ case [31]. This information on cold reaction valleys (target-projectile combinations), optimized in terms of the calculated scattering potentials, for smallest interaction barrier and largest interaction radius, show that the spherical ^{48}Ca and ^{54}Ti induced reactions on various deformed actinides are still the first and second best cold fusion reactions for Z = 112 and 114 compound systems, as was the case for $\phi = 0^0$ collisions [31]. Note that both of these are co-planar reactions since one of the reaction partners is a spherical nucleus. For the deformed + deformed combination, involving non-coplanar ($\phi_c \neq 0^0$) collisions, the new pairs ^{226}Ra+^{60}Cr and ^{234}U+^{58}Ti of cold fusion reactions are obtained, respectively, for Z = 112 and 114 compound systems.

REFERENCES

1. J. Maruhn and W. Greiner, Phys. Rev. Lett. **32**, 548 (1974).
2. R. K. Gupta, W. Scheid and W. Greiner, Phys. Rev. Lett. **35**, 353 (1975).
3. U. Quade, *et al., Lecture Notes in Physics* **158**, 40 (1981).
4. F. J. Gönnenwein, *Proc. Int. Conf. on Nucl. Data for Basic and Applied Science*, Santa Fe, New Mexico, USA, 1985.
5. A. Săndulescu, D. N. Poenaru and W. Greiner, Sov. J. Part. Nucl. **11**, 528 (1980).
6. H. J. Rose and G. A. Jones, Nature **307**, 245 (1984).
7. H. J. Fink, W. Greiner, R. K. Gupta, S. Liran, H. J. Maruhn, W. Scheid and O. Zohni, *Proc. Int. Conf. on Reactions between Complex Nuclei*, Nashville**,** USA**.** (North Holland), (1974), p. 21.
8. A. Săndulescu, R. K. Gupta, W. Scheid and W. Greiner, Phys. Lett. **60 B**, 225 (1976).
9. R. K. Gupta, A. Săndulescu and W. Greiner, Phys. Lett. **67 B**, 257 (1977).
10. K. Gupta, C. Pírvulescu, A. Săndulescu and W. Greiner, Z. Physik **A 283**, 217 (1977).
11. R. K. Gupta, A. Săndulescu and W. Greiner, Z. Naturforsch **32a**, 704 (1977).
12. R. K. Gupta, Sov. J. Part. Nucl. **8**, 289 (1977).
13. S Hofmann, *et al*, Z. Phys. **A 350**, 277 (1995).
14. S Hofmann, *et al*, Z. Phys. **A 350**, 281 (1995).
15. V Ninov, *et al*, Z. Phys. **A 356**, 11 (1996).
16. Yu. A. Lazarev, *et al*, Phys. Rev. Lett. **73**, 624 (1994).
17. G. M. Ter-Akopian, *et al*, Phys. Rev. Lett. **73**, 1477 (1994).
18. E. K. Hulet, *et al*, Phys. Rev. Lett. **56**, 313 (1986).
19. G. M. Ter-Akopian, *et al*, Phys. Rev. Lett. **77**, 32 (1996).
20. W. Mollenkopf, *et al*, J. Phys. G: Nucl. Part. Phys. **18**, L203 (1992).
21. S. K. Arun, R. K. Gupta, B. B. Singh, S. Kanwar and M. K. Sharma, Phys. Rev. C **79**, 064616 (2009).
22. S. K. Arun, R. K. Gupta, S. Kanwar, B. B. Singh and M. K. Sharma, Phys. Rev. C **80**, 034317 (2009).
23. G. Sawhney, M. K. Sharma and R. K. Gupta, Phys. Rev. C **83**, 064610 (2011).
24. M. Manhas and R. K. Gupta, Phys. Rev. C **72**, 024606 (2005).
25. R. K. Gupta, M. Balasubramaniam, R. Kumar, N. Singh, M. Manhas and W. Greiner, J. Phys. G: Nucl. Part. Phys. **31**, 631 (2005).
26. *Heavy elements and related new phenomena* edited by W. Greiner and R. K. Gupta (World Scientific Publication, 1999) Vols. I and II.
27. *Physics of Particles, Nuclei and Materials-Recent Trends,* edited by R. K. Gupta (Narosa Publishing House, 2002).
28. P. Möller, *et al.*, At. Nucl. Data Tables **59**, 185 (1995).
29. G. Audi and A. H. Wapstra, Nucl. Phys. **A 595**, 4 (1995).
30. R. K. Gupta, N. Singh, and M. Manhas, Phys. Rev. C **70**, 034608 (2004).
31. R. K. Gupta, M. Manhas and W. Griener, Phys. Rev. C **73** 054307 (2006); R. K. Gupta, M. Manhas, G. Münzenberg and W. Greiner, Phys. Rev. C **72**, 014607 (2005).
32. M. Manhas, R. K. Gupta, Q. Li, S. K. Patra and W. Griener, Phys. Rev. C **74** 034603 (2006).
33. Yu.Ts. Oganessian, *et al.*, Phys. Rev. C **69**, 054607 (2004).
34. Yu.Ts. Oganessian, *et al.* ,Phys. Rev. C 70, 064609 (2004).
35. M. Manhas, *Ph.D. thesis, Panjab University, Chandigarh (India),* (2007), unpublished.